Decarbonylation of MgO-Supported PtRh₅ Clusters Characterized by Infrared and Extended X-ray Absorption Fine Structure Spectroscopies

O.-B. Yang, M. Shirai, W. A. Weber, and B. C. Gates*

Department of Chemical Engineering and Materials Science, University of California, Davis, California 95616

Received: March 26, 1998; In Final Form: June 22, 1998

[PtRh₅(CO)₁₅]⁻ was synthesized from RhCl₃, Na₂PtCl₆, and CO in methanol slurried with MgO powder; after removal of the methanol, [PtRh₅(CO)₁₅]⁻ remained adsorbed on the MgO surface. In addition to the metal carbonyl clusters, X-ray absorption near edge spectra indicated the presence of cationic rhodium species on the MgO surface. When the sample was treated in He or H₂, decarbonylation took place, accompanied by temperature-dependent aggregation of the metals, as indicated by infrared spectra and EXAFS spectra measured at both the Rh K and Pt L$_{III}$ edges. The resultant decarbonylated clusters and aggregates were bimetallic and not significantly segregated into separate metals. The smallest supported bimetallic clusters incorporated only about 6−10 atoms each; on average—these are among the smallest supported bimetallic clusters yet reported. The smallest supported clusters were not fully decarbonylated; complete decarbonylation resulted in aggregation of the metal without significant segregation of the metal. The EXAFS data indicate that the aggregates had rhodium-rich cores, with the platinum concentrated near the surfaces.

Introduction

Industrially important supported metal catalysts include bimetallics[1−3] (e.g., those containing Pt and Rh, which are used for the abatement of automobile exhaust gases.)[1] Pt−Rh clusters have been prepared in the pores of NaY zeolite by ion exchange with an aqueous solution containing Pt(NH₃)₄Cl₂ and Rh(NH₃)₅-Cl₃ followed by calcination and reduction.[4−6] Similarly, Pt−Rh alloy particles have been formed from platinum and rhodium salts on SiO₂ and on γ-Al₂O₃.[7−9] The conventional preparation method consisting of calcination of supported salts followed by reduction may lead to aggregation with segregation of the metals, in part because the two metals are not oxidized or reduced with equal facility. Because the precursor platinum and rhodium salts are separate, the formation of bimetallic structures on the support is difficult to control. And because the supported bimetallics are nonuniform in composition and structure, the determination of structure-catalytic property relationships is difficult.

To simplify matters, researchers have used molecular supported bimetallic clusters as precursors of supported catalysts.[10] Here we report spectroscopic results characterizing the evolution of platinum and rhodium surface species as molecular bimetallic precursors were converted into supported bimetallic clusters. Catalytic properties of the samples are to be reported separately.[11]

Our goal was to treat samples formed from [PtRh₅(CO)₁₅]⁻ and MgO in He or H₂ at elevated temperature, leading to the removal of carbonyl ligands with minimal aggregation and segregation of the metals. The foundation for understanding the surface chemistry of the preparation of the organometallic precursor is its known solution organometallic chemistry, which has been investigated along with that of other bimetallic anionic carbonyls;[12−15] Xu et al.[16] prepared [PtRh₅(CO)₁₅]⁻ on MgO. The bimetallic species and their decarbonylation have been characterized by infrared and extended X-ray absorption fine structure (EXAFS) spectroscopies.

Experimental Section

Materials and Sample Preparation. Syntheses and sample transfers were carried out with exclusion of air and moisture on a double-manifold Schlenk vacuum line and in a N₂-filled glovebox (AMO-2032, Vacuum Atmospheres Co.). Preparation of the precursor [PtRh₅(CO)₁₅]⁻ on MgO was as described by Xu et al.[16]

Samples were decarbonylated in He or H₂ flowing at 60 mL (NTP)/min at 1 atm and temperatures of 125, 175, and 400 °C or 125, 200, 275, and 400 °C, respectively; some samples were recarbonylated in CO flowing at 1 atm in an infrared cell or an EXAFS cell. The precursor bimetallic carbonyls were oxidized in air at temperatures up to 175 °C.

Extraction of Metal Carbonyls from MgO. Surface-bound bimetallic carbonyls were extracted from the surface of MgO as the solid sample was brought in contact with a solution of bis(triphenylphosphine)nitrogen(1+) chloride ([PPN][Cl]) in methanol under N₂, as described elsewhere.[16]

Infrared Spectroscopy. Transmission infrared spectra of the samples (powder or liquid) were recorded with a Bruker IFS-66V spectrometer, as described previously.[17]

X-ray Absorption Spectroscopy. EXAFS and X-ray absorption near edge spectroscopy (XANES) experiments characterizing the solid samples at the Rh K edge (23220 eV) and at the Pt L$_{III}$ edge (11564 eV) were performed on beam line 2-3 of the Stanford Synchrotron Radiation Laboratory (SSRL) at the Stanford Linear Accelerator Center, Stanford, CA, and on beam line X-11A of the National Synchrotron Light Source (NSLS) at Brookhaven National Laboratory, Upton, NY. The storage rings operated with electron energies of 3 GeV at SSRL and 2.5 GeV at NSLS; the beam current was 70−100 mA at SSRL and 140−240 mA at NSLS.

---

* To whom correspondence should be addressed.

TABLE 1: Crystallographic Data Characterizing Reference Compounds and Fourier Transform Ranges Used in EXAFS Data Analysis[a]

| ref sample | shell | crystallographic data | | | Fourier transform[a] | | |
		N	r, Å	ref	Δk, Å^{-1}	Δr, Å	n
Rh foil	Rh−Rh	12	2.687	25	2.86−19.60	1.62−3.12	3
RhPt[b]	Rh−Pt	8	2.69	this work	2.70−19.96	0.16−5.00	1
RhMg[b]	Rh−Mg	1	1.70	this work	1.0−20.0	0−8.0	0
Rh$_2$O$_3$	Rh−O	6	2.050	26	2.67−15.69	0.00−2.10	2
[Ru$_3$(CO)$_{12}$]	Rh−C	4	1.910	27	3.71−14.80	0.95−1.87	1
	Rh−O*	4	3.050	27	3.75−14.80	1.90−3.11	2
PtRh[b]	Pt−Rh	8	2.69	this work	2.51−19.91	0.12−4.37	1
Na$_2$Pt(OH)$_6$	Pt−O	6	2.05	28	1.4−17.7	0.5−2.0	3
[Ir$_4$(CO)$_{12}$]	Ir−C	3	1.87	29	2.8−16.5	1.1−2.0	3

a Notation: *N*, coordination number for absorber−backscatterer pair; *R*, distance; Δk, limits used for forward Fourier transformation (*k* is the wave vector); Δr, limits used for shell isolation (*r* is distance); *n*, power of *k* used for Fourier transformation. *b* Calculated using FEFF 4.06, ref 19.

TABLE 2: Summary of EXAFS Analysis: Fitted *k*-Range and *r*-Range, Number of Scans, and Standard Deviation in EXAFS Function Characterizing PtRh/MgO Samples Prepared from [PtRh$_5$(CO)$_{15}$]$^-$

| treatment conditions | | no. of scans | absorption edge | k range, Å^{-1} | r range, Å |
gas	temperature °C				
none	none	3	Pt L$_{III}$	3.6−12.0	0−5
He	125	4	Pt L$_{III}$	3.7−11.5	0−5
He	175	4	Pt L$_{III}$	4.1−11.5	0−5
He	400	4	Pt L$_{III}$	4.1−11.5	0−5
H$_2$	125	4	Pt L$_{III}$	4.1−11.5	0−5
H$_2$	200	3	Pt L$_{III}$	4.1−11.5	0−5
H$_2$	275	4	Pt L$_{III}$	4.1−11.5	0−5
H$_2$	400	3	Pt L$_{III}$	4.1−11.5	0−5
none	none	5	Rh K	3.9−11.8	0−5
He	125	3	Rh K	4.1−12	0−5
He	175	3	Rh K	4.1−12	0−5
He	400	4	Rh K	4.1−12	0−5
H$_2$	125	3	Rh K	4.1−12	0−5
H$_2$	200	3	Rh K	4.1−12	0−5
H$_2$	275	2	Rh K	4.1−12	0−5
H$_2$	400	2	Rh K	4.1−12	0−5

The experimental methods for collecting transmission EXAFS and XANES data at the Rh K and Pt L$_{III}$ edges are similar to those reported.[17,18]

EXAFS Data and Analysis

EXAFS Reference Data. The EXAFS data were analyzed with experimentally determined reference files for Rh−Rh, Rh−O$_s$ (O$_s$ is support oxygen), Rh−C, Rh−O* (O* is carbonyl oxygen), Pt−Pt, Pt−O$_s$, Pt−C, and Pt−O* contributions. Pt−Rh, Rh−Pt, and Rh−Mg interactions were analyzed with phase shifts and backscattering amplitudes obtained from EXAFS functions calculated theoretically with the FEFF program.[19] Details of the preparation of the reference files are stated elsewhere,[20−24] and the parameters used to extract these files from the EXAFS data are summarized in Table 1.

[PtRh$_5$(CO)$_{15}$]$^-$/MgO. EXAFS data were obtained for the sample formed after the removal of methanol from the [PtRh$_5$(CO)$_{15}$]$^-$/MgO slurry, inferred to consist predominantly of [PtRh$_5$(CO)$_{15}$]$^-$ supported on MgO.[16] Each sample was scanned three times at the Pt L$_{III}$ edge and three times at the Rh K edge. The EXAFS data at the Rh K edge were fitted with one Rh−Rh contribution, one Rh−O$_s$ contribution, two Rh−C contributions, and one Rh−O* contribution. The EXAFS data at the Pt L$_{III}$ edge were fitted with one Pt−Rh contribution, one Pt−O$_s$ contribution, one Pt−C contribution, and one Pt−O* contribution. Thus, the number of parameters used to fit the
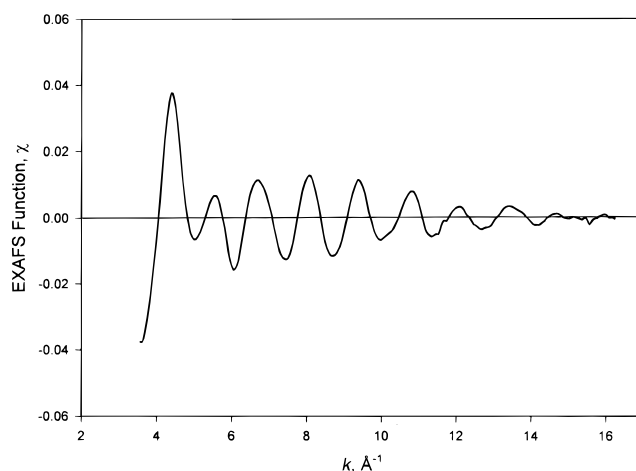

Figure 1. Rh K-edge raw EXAFS data characterizing MgO-supported Pt−Rh clusters formed by treatment in He at 175 °C of MgO-supported sample incorporating [PtRh$_5$(CO)$_{15}$]$^-$.

data in this main-shell analysis was 20 for the Rh K-edge data and 16 for the Pt L$_{III}$-edge data; the statistically justified number, estimated on the basis of the Nyquist theorem,[30] was at least 26 for the data at each edge. The *k*- and *r*-ranges (*r* is distance) used in the data fitting are summarized in Table 2.

He- and H$_2$-Treated Samples (Decarbonylated Samples). *A. Analysis of Rh-Edge Data.* EXAFS data were also obtained for the samples formed by treatment of the precursor bimetallic carbonyls in He or H$_2$ at temperatures of 125, 175, and 400 °C or 125, 200, 275, and 400 °C, respectively. Each normalized EXAFS function was obtained from averaged EXAFS spectra (Table 2) by a cubic spline background subtraction and normalized by division by the edge height (e.g., Figure 1). Strong oscillations were observed for each sample in the intermediate and higher ranges of the wave vector *k* (8 < *k* < 16 Å^{-1}), consistent with metal−metal interactions and the presence of metal clusters or particles.

Using a difference file technique,[24,31] the EXAFS data characterizing each of the samples treated at temperatures <400 °C were fitted for a Rh−Rh contribution, and the Rh-low-*Z* contributions were approximated by one Rh−O$_s$ contribution (at about 2.1 Å), one Rh−C contribution (at about 1.9 Å), one Rh−O* contribution (at about 3 Å), and one Rh−Mg contribution (at about 1.7 Å). The difference file was fitted for these contributions until good agreement was found between the raw data and the fit with k^0 weighting in *r* space. The final Rh−Rh contribution showed very good agreement with the residual data not only for k^0 weighting but also for k^1, k^2, and k^3 weightings. The EXAFS data characterizing the samples formed by decar-

MgO-Supported PtRh Clusters

J. Phys. Chem. B, Vol. 102, No. 44, 1998 **8773**

TABLE 3: Summary of Infrared Spectra: ν_{CO} Stretching Frequencies Characterizing Platinum−Rhodium Carbonyls in Solution and on MgO

sample	terminal CO stretching frequency, cm^{-1} [a]	bridging CO stretching frequency, cm^{-1}	ref
[PtRh$_5$(CO)$_{15}$]$^-$ in THF	2082 vw, 2038 s, 2011 m	1791 ms	13
supernatant [PtRh$_5$(CO)$_{15}$]$^-$ in CH$_3$OH	2082 vw, 2041 s, 2009 m	1790 ms	this work
[PtRh$_5$(CO)$_{15}$]$^-$ on MgO (1A)	2082 vw, 2041 s, 2015 ms	1812 br	this work
sample extracted from sample 1A with [PPN][Cl] in CH$_3$OH	2082 vw, 2041 s, 2009 m, 1982 w	1790 ms	this work
1A after decarbonylation treatment in H$_2$ at 200 °C	2015 ms, 1945 ms		this work
1A after decarbonylation treatment in He at 120 °C	2092 m, 2024 m		this work
sample formed by recarbonylation at 275 °C after decarbonylation treatment of sample 1A in H$_2$ at 275 °C	2057 ms, 2026 br, 1993 br	1843 br	this work
sample formed by recarbonylation at 175 °C after decarbonylation treatment of sample 1A in He at 175 °C	2092 m, 2057 ms, 2026 s	1832 br	this work
1A treated in O$_2$ at 25 °C for 10 min	2084 ms, 2046 ms, 2015 ms	1818 br	this work
1A treated in O$_2$ at 100 °C for 1 min	2091 ms, 2021 ms		this work

[a] vw = very weak. m = medium. ms = medium strong. s = strong. br = broad.
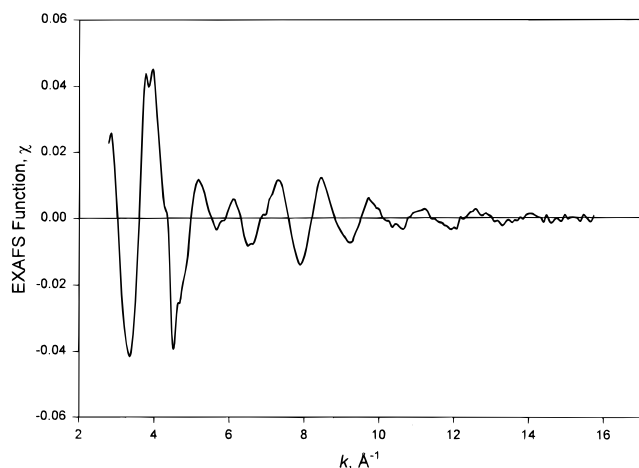
Figure 2. Pt L$_{III}$-edge raw EXAFS data characterizing MgO-supported Pt−Rh clusters formed by treatment in He at 175 °C of MgO-supported sample incorporating [PtRh$_5$(CO)$_{15}$]$^-$.

bonylation of the precursor supported metal carbonyls at 400 °C were fitted simply with a Rh−Rh contribution and a Rh−O$_s$ contribution, with each spectrum dominated by the Rh−Rh contribution.

B. Analysis of Pt-Edge Data. The normalized EXAFS functions were obtained from averaged EXAFS spectra (Table 2) by a cubic spline background subtraction and normalized by division by the edge height (e.g., Figure 2). The data characterizing each of the samples referred to in the preceding section indicate strong oscillations in the intermediate and higher ranges of the wave vector ($8 < k < 16$ Å^{-1}), consistent with metal−metal contributions and the presence of metal clusters or particles. However, because of the low platinum loading, the signal-to-noise ratio was low, and the high-k region ($k > 12$ Å^{-1}) was typically dominated by noise.

With the same method described above, the data characterizing each sample were fitted for Pt−Rh, Pt−C, Pt−O*, and Pt−O$_s$ contributions. The number of parameters used to fit the data for each sample ranged from 8 to 16; the statistically justified number, estimated on the basis of the Nyquist theorem,[30] is approximately 28 for each sample.

Results

[PtRh$_5$(CO)$_{15}$]$^-$ Supported on MgO. After removal of the methanol solution from the slurry containing MgO and [PtRh$_5$(CO)$_{15}$]$^-$, the infrared spectrum of the resultant solid matched that of the sample prepared by Xu et al.[16] (Table 3). The species extracted into solution from the solid had the same

ν_{CO} infrared fingerprint as [PtRh$_5$(CO)$_{15}$]$^-$ (Table 3). These results confirm those of Xu et al.[16] and support the conclusion that at least some of the [PtRh$_5$(CO)$_{15}$]$^-$ clusters remained intact after synthesis in the slurry and adsorption on MgO.

The raw EXAFS data characterizing the Rh K edge of the MgO-supported [PtRh$_5$(CO)$_{15}$]$^-$ (Figure 3) were fitted initially with only a Rh−C contribution, a Rh−O contribution, and a Rh−O* contribution, but the fit was poor for values of $k > 9$ Å^{-1}; consequently, a Rh−Rh contribution was included, improving the fit and indicating the presence of clusters. The structural parameters used to fit the data are summarized in Table 4.

To illustrate the goodness of the fits, comparisons of the raw data and the fits in k space and in r space are shown in Figure 3A and B, respectively. A comparison of the fitted Rh−Rh contribution with the residual spectrum formed by subtraction of the Rh-low-Z contributions from the raw EXAFS function is shown in Figure 3C. Similarly, the fitted Rh-low-Z contributions (Table 4) are compared in Figure 3D with the residual spectrum determined by subtraction of the Rh−Rh contribution from the raw EXAFS function. These comparisons show that the Rh−Rh and Rh-low-Z contributions were fitted satisfactorily.

The raw Pt L$_{III}$ EXAFS data characterizing MgO-supported [PtRh$_5$(CO)$_{15}$]$^-$ are shown in Figure 4. The data quality is not high because the platinum loading was low; because the platinum signal intensity was low, the nonuniformity of the sample thickness affected the spectrum. Nonetheless, the results are sufficient to provide some structural information about the near neighbors around platinum. Only with the inclusion of a Pt−Rh contribution at about 2.83 Å could the data be fitted satisfactorily in the high-k range ($8 < k < 12$ Å^{-1}). The structural parameters used to fit the data are summarized in Table 4.

To illustrate the goodness of the fits, comparisons of the raw data and the fits in k space and in r space are shown in Figure 4A and B, respectively. A comparison of the fitted Pt−Rh contribution with the residual spectrum formed by subtraction of the Pt-low-Z contributions from the raw EXAFS function is shown in Figure 4C. Similarly, the fitted Pt-low-Z contributions [Pt−O$_s$, Pt−O*, and Pt−C] are compared in Figure 4D with the residual spectrum formed by subtraction of the Rh−Rh contribution from the raw EXAFS function. These comparisons show that the Pt−Rh and Pt-low-Z contributions were fitted satisfactorily.

The Rh K-edge XANES of the sample incorporating [PtRh$_5$(CO)$_{15}$]$^-$ with MgO is compared with the Rh K-edge XANES of [Rh$_6$(CO)$_{16}$] supported on NaY zeolite (Figure 5).[17,32] The comparison shows that the rhodium in the former sample

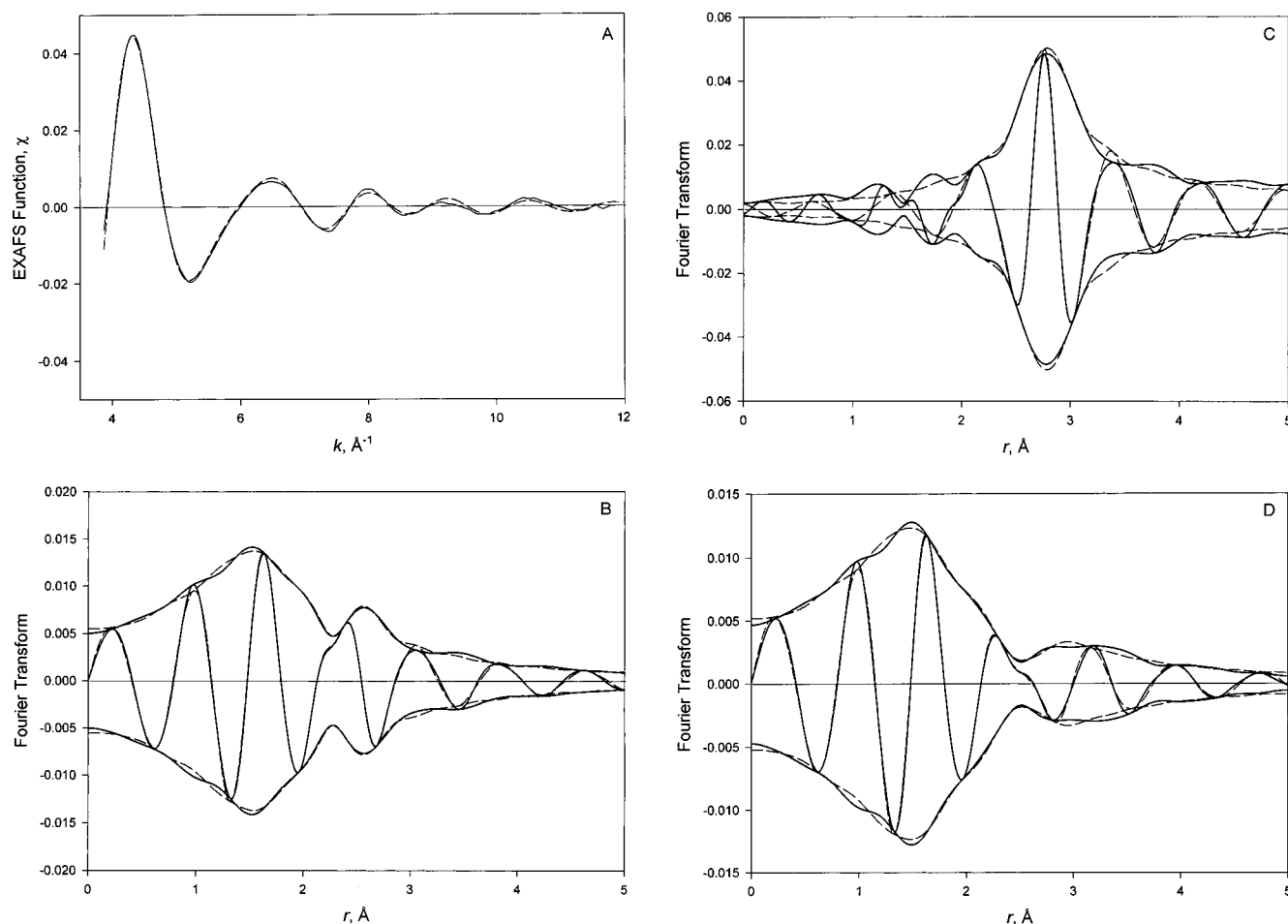**Figure 3.** Results of Rh K-edge EXAFS analysis characterizing the sample prepared by removal of solution from the slurry containing MgO and [PtRh$_5$(CO)$_{15}$]$^-$: (A) raw EXAFS function (solid line) and sum of the calculated Rh−Rh + Rh−O$_s$ + Rh−C (two different distances) + Rh−O* contributions (dashed line). (B) Imaginary part and magnitude of Fourier transform (unweighted, $\Delta k = 3.9−11.8$ Å^{-1}) of raw EXAFS function (solid line) and sum of the calculated Rh−Rh + Rh−O$_s$ + Rh−C + Rh−O* contributions (dashed line). (C) Residual spectrum illustrating the Rh−Rh contribution; imaginary part and magnitude of Fourier transform (unweighted, Rh−Rh phase- and amplitude-corrected, $\Delta k = 3.9−11.8$ Å^{-1}) of raw EXAFS data minus calculated Rh−O$_s$ + Rh−C + Rh−O* contributions (solid line) and calculated Rh−Rh contribution (dashed line). (D) Residual spectrum illustrating the Rh-low-Z interactions; imaginary part and magnitude of Fourier transform (unweighted, $\Delta k = 3.9−10$ Å^{-1}) of raw EXAFS data minus calculated Rh−Rh contribution (solid line) and calculated Rh−O$_s$ + Rh−C + Rh−O* contributions (dashed line).

TABLE 4: EXAFS Results Characterizing the Sample Incorporating [PtRh$_5$(CO)$_{15}$]$^-$ Adsorbed on MgO^a

absorption edge	backscatterer	N	R, Å	$\Delta\sigma^2$, Å^2	ΔE_0, eV
Rh K	Rh	4.0	2.76	0.008 38	−1.6
	C^b	2.1	2.08	0.000 00	2.2
	C^c	2.1	1.94	0.010 00	14.6
	O*	3.7	3.30	0.015 00	2.3
	O	2.9	2.31	0.008 00	−20.0
Pt L$_{III}$	Rh	2.9	2.83	0.002 58	0.7
	O	3.4	2.11	0.00625	−4.0
	C	4.0	1.88	0.008 27	−13.5
	O*	3.5	2.96	0.012 29	0.3

^{a} Notation: N, coordination number characterizing absorber-backscatterer pair; R, distance; $\Delta\sigma^2$, Debye−Waller factor; ΔE_0, inner potential correction; O* refers to carbonyl oxygen.

is more electron deficient than rhodium in the latter. As the infrared and EXAFS results indicate the presence of [PtRh$_5$-(CO)$_{15}$]$^-$ on MgO, we interpret the XANES data to indicate the presence of cationic rhodium on the support as well. These species were evidently not extracted with the anionic clusters.

Decarbonylation of Sample Containing [PtRh$_5$(CO)$_{15}$]$^-$ on MgO: Characterization by Infrared Spectroscopy. Decarbonylation of the sample containing [PtRh$_5$(CO)$_{15}$]$^-$ on MgO in the presence of He was indicated by the decrease in intensity

of the 1814-cm^{-1} band, associated with face-bridging CO ligands (Figure 6); this band disappeared before the temperature reached 90 °C. Correspondingly, the ν_{CO} bands associated with terminal CO ligands, characterized by a strong absorption at 2041 cm^{-1}, were transformed into a doublet at 2091 and 2023 cm^{-1} (Figure 6). Decarbonylation was nearly complete at 175 °C.

When decarbonylation of the supported clusters was carried out in the presence of H$_2$ instead of He, the infrared spectrum was characterized by decreasing intensities of the terminal ν_{CO} bands accompanied by shifts to lower wavenumbers with increasing temperature (Figure 7). The face-bridging ν_{CO} band at 1814 cm^{-1} had disappeared before the temperature reached 175 °C. Decarbonylation was nearly complete at 275 °C.

Characterization of Decarbonylated Clusters by EXAFS Spectroscopy. *A. Rh K-Edge Data.* The raw EXAFS data characterizing the Rh K edges of the samples treated in He at 125, 175, or 400 °C or in H$_2$ at 125, 200, 275, or 400 °C show oscillations up to values of k equal to about 12 Å^{-1} or greater, depending on the gas phase and the temperature of decarbonylation treatment. The Fourier transforms of the raw data characterizing these samples are shown in Figure 8A and B. Fitting of the data for each sample indicated a Rh−Rh contribution at about 2.7 Å. An attempt was made to include
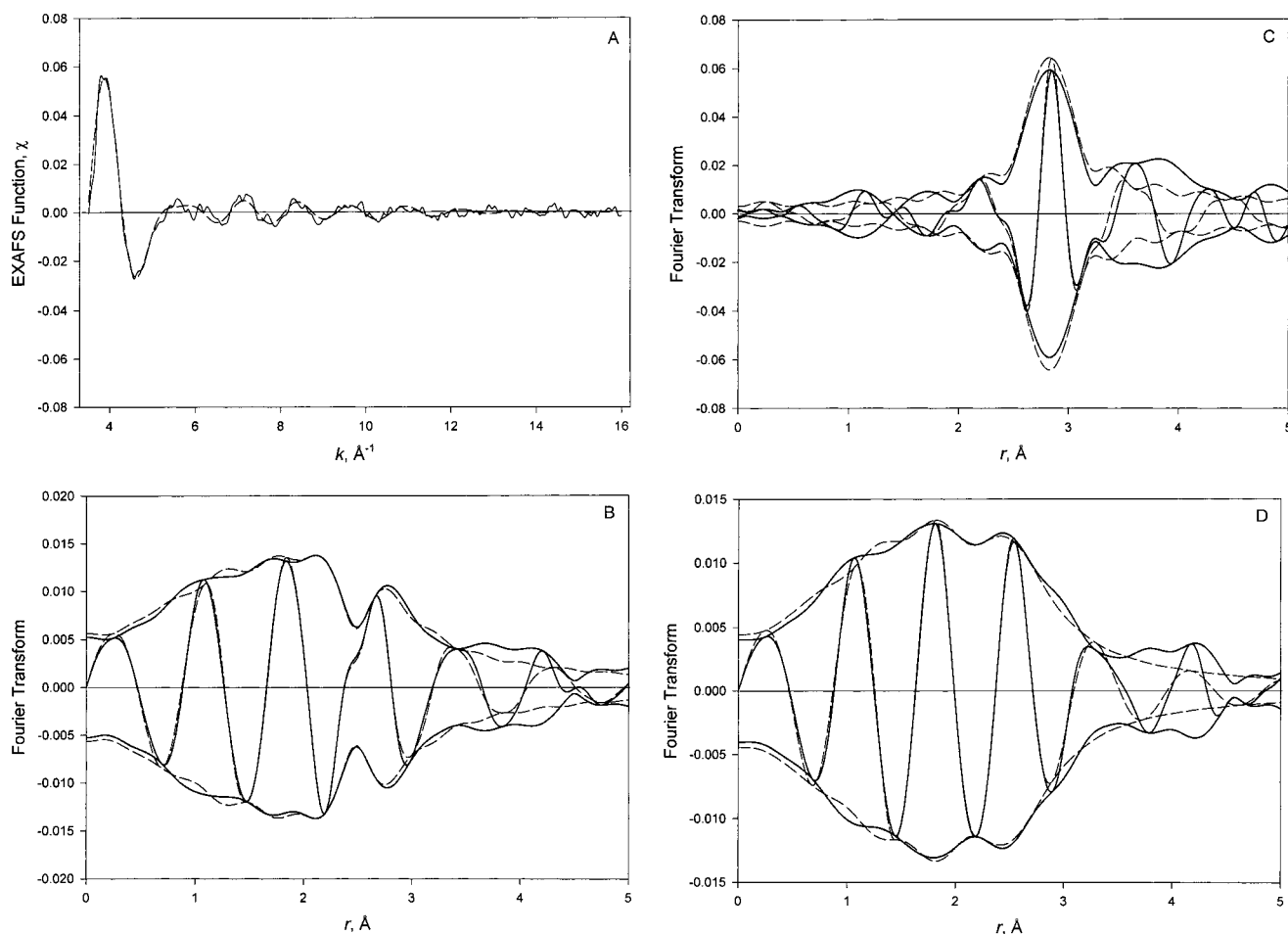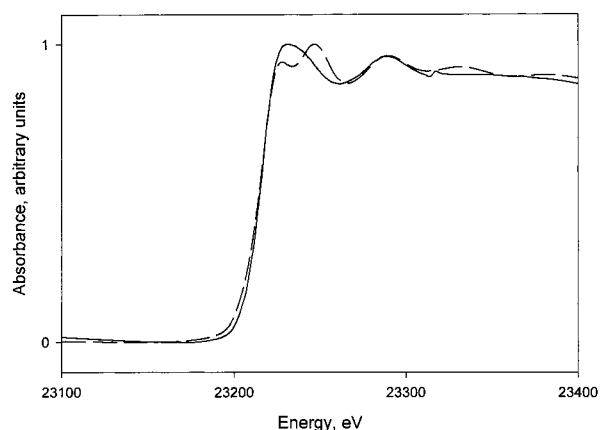
Figure 4. Results of Pt L$_{III}$-edge EXAFS analysis characterizing the sample prepared by removal of solution from the slurry containing MgO and [PtRh$_5$(CO)$_{15}$]$^-$: (A) raw EXAFS function (solid line) an sum of the calculated Pt−Rh + Pt−O$_s$ + Pt−C + Pt−O* contributions (dashed line). (B) Imaginary part and magnitude of Fourier transform (unweighted, $\Delta k = 3.6–12$ Å^{-1}) of raw EXAFS function (solid line) and sum of the calculated Pt−Rh + Pt−O$_s$ + Pt−C + Pt−O* contributions (dashed line). (C) Residual spectrum illustrating the Pt−Rh contribution; imaginary part and magnitude of Fourier transform (unweighted, Pt−Rh phase- and amplitude-corrected, $\Delta k = 3.6–12$ Å^{-1}) of raw EXAFS data minus calculated Pt−O$_s$ + Pt−C + Pt−O* contributions (solid line) and calculated Pt−Rh contribution (dashed line). (D) Residual spectrum illustrating the Pt-low-Z contributions; imaginary part and magnitude of Fourier transform (unweighted, $\Delta k = 3.9–10$ Å^{-1}) of raw EXAFS data minus calculated Pt−Rh contribution (solid line) and calculated Pt−O$_s$ + Pt−C + Pt−O* contributions (dashed line).

Figure 5. Comparison of the Rh K-edge X-ray absorption data (XANES spectra) characterizing NaY zeolite-supported [Rh$_6$(CO)$_{16}$] (dashed line)[33] and the sample prepared by removal of solution from the slurry containing MgO and [PtRh$_5$(CO)$_{15}$]$^-$ (solid line).

a Rh−Pt contribution (at about 2.7 Å) in the fit, but it was not indicated by the data.

In addition to the Rh−Rh contribution, the data were fitted with a Rh−O contribution at about 2.1 Å and, in the samples that were not fully decarbonylated, a Rh−C contribution at about

1.9 Å, and a Rh−O* contribution at about 3.1 Å. The Rh−C contribution decreased with increasing temperature of decarbonylation whether the treatment gas was He or H$_2$, consistent with increasing decarbonylation of the sample with increasing temperature. However, the sum of these three contributions is only an approximation of the Rh-low-Z contributions; the data are not sufficient to determine them separately with confidence, and only the data characterizing the metal−metal contribution are shown (Table 5).

The ratio of the magnitude of the Fourier transform of the raw EXAFS data characterizing the decarbonylated sample formed at 275 °C in He to that of the sample formed at 125 °C in He at the value of r characterizing the metal−metal contribution (about 2.7 Å) is about 3:1. Likewise, the equivalent ratio of the magnitude of the Fourier transform of the raw EXAFS data characterizing the decarbonylated sample formed at 275 °C in H$_2$ to that of the sample formed at 125 °C in H$_2$ is about 3:1. These results show increasing metal−metal contributions as a result of the decarbonylation process, consistent with aggregation of the metal.

EXAFS data characterizing supported clusters formed by decarbonylation in He at temperatures exceeding 125 °C showed little or no evidence of Rh−C and Rh−O* contributions, as evidenced by a Rh−C coordination number less than 1 (data

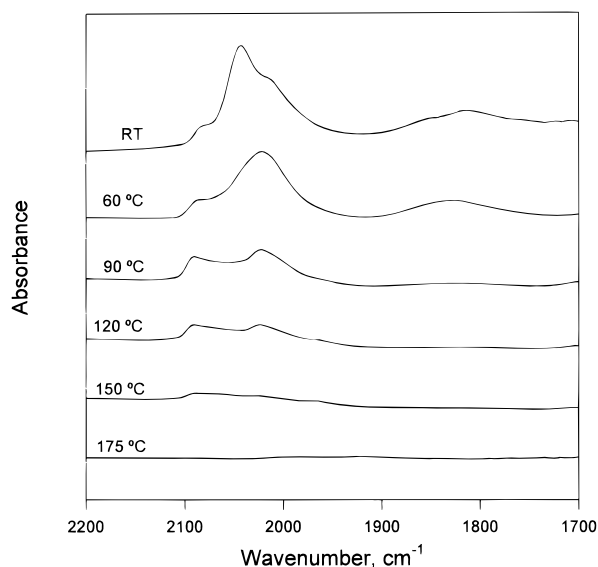**8776** *J. Phys. Chem. B, Vol. 102, No. 44, 1998*

Yang et al.

Figure 6. Infrared spectra of the sample prepared by removal of solution from the slurry containing MgO and [PtRh₅(CO)₁₅]⁻ and its subsequent treatments in He at the temperatures shown.
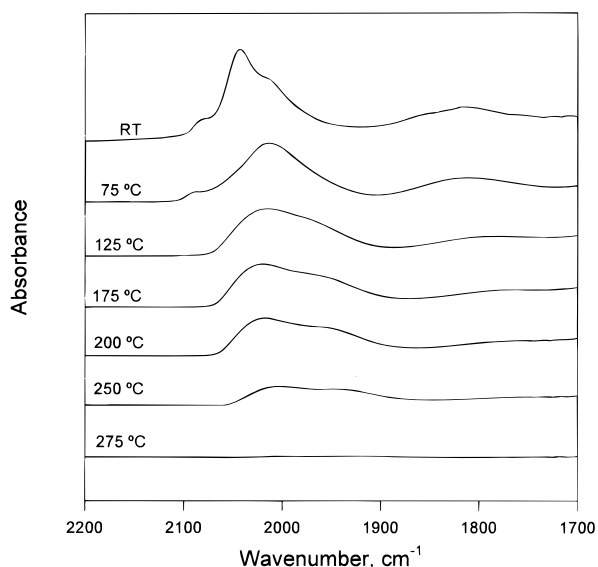

Figure 7. Infrared spectra of the sample prepared by removal of solution from the slurry containing MgO and [PtRh₅(CO)₁₅]⁻ and its subsequent treatments in H₂ at the temperatures shown.

not shown). Samples decarbonylated in H₂ at temperatures less than 275 °C showed significant Rh−C and Rh−O* contributions.

B. Pt L_III-Edge Data. The raw Pt L_III-edge data characterizing the decarbonylated samples mentioned in the preceding paragraph show oscillations up to values of *k* equal to about 12 Å⁻¹ or greater, depending on the gas phase and the temperature of decarbonylation. Because the platinum content of the sample was low, the data quality is low relative to that of the Rh K-edge data, and the results are sufficient only to provide trends in the Pt−Rh coordination numbers and evidence of the existence of interactions of platinum with low-*Z* scatterers. Consistent with the conclusion that the surface species included metal carbonyls, the Pt L_III-edge EXAFS data characterizing the MgO-supported sample indicate the presence of both Pt−C and Pt−O contributions. Furthermore, a Pt−Rh contribution was fitted with a coordination number of 2.9 at a distance of 2.83 Å. The Fourier transforms of the raw EXAFS data are shown in Figures 9A

TABLE 5: EXAFS Results Characterizing the Metal−Metal Contributions of Platinum−Rhodium Clusters and Particles Formed by Decarbonylation of the Sample Formed From [PtRh₅(CO)₁₅]⁻ Supported on MgO[a]

gas	temperature, °C	absorption edge	backscatterer	N	R, Å	Δσ², Å²	ΔE₀, eV
He	125	Rh K	Rh	4.5	2.68	0.002 31	12.5
He	175	Rh K	Rh	6.0	2.68	0.002 56	19.7
He	400	Rh K	Rh	10.0	2.66	0.002 35	4.2
H₂	125	Rh K	Rh	5.2	2.71	0.004 36	13.0
H₂	200	Rh K	Rh	6.0	2.66	0.004 61	16.2
H₂	275	Rh K	Rh	9.1	2.67	0.003 15	7.7
H₂	400	Rh K	Rh	8.7	2.67	0.002 01	2.4
He	125	Pt L_III	Rh	3.5	2.73	0.002 03	20.0
He	175	Pt L_III	Rh	3.1	2.76	0.001 38	7.90
He	400	Pt L_III	Rh	4.7	2.76	−0.002 19	−10.9
H₂	125	Pt L_III	Rh	3.9	2.82	0.000 90	1.7
H₂	200	Pt L_III	Rh	3.8	2.80	0.002 00	2.8
H₂	275	Pt L_III	Rh	5.0	2.74	0.000 00	2.7
H₂	400	Pt L_III	Rh	5.0	2.76	0.000 00	−4.0

[a] Notation as in Table 4.

and 10A. The structural parameters used to fit the Pt−Rh contribution characterizing each sample are summarized in Table 5.

Figures 9B and 10B show the Fourier transforms of the raw Pt L_III-edge EXAFS data characterizing the samples formed in He and in H₂, respectively, phase and amplitude corrected on the basis of data characterizing platinum foil. The Fourier transforms include no distinct positive peaks in the imaginary part near 2.7 Å, in contrast to the Fourier transforms of the same data that were phase and amplitude corrected on the basis of data characterizing Pt−Rh interactions predicted by FEFF (Figures 9A and 10A).[19] This comparison shows that, although a weak Pt−Pt contribution may exist, the predominant interaction of platinum was with rhodium.

The ratio of the magnitude of the Fourier transform of the raw EXAFS data characterizing the decarbonylated sample formed in He at 275 °C to that of the sample formed in He at 125 °C (at about 2.7 Å) is about 2:1. Likewise, the ratio of the magnitude of the Fourier transform of the raw EXAFS data characterizing the decarbonylated sample formed in H₂ at 275 °C to that of the sample formed in H₂ at 125 °C is about 2:1 (Figures 9A and 10A). Again, the results indicate aggregation of the metal.

Recarbonylation of Decarbonylated Clusters. With CO at 1 atm flowing through the infrared cell containing the decarbonylated clusters supported on MgO, the temperature was ramped from room temperature as infrared spectra were recorded. Recarbonylation at 25 °C of the sample that had been treated in He at 175 °C resulted in a spectrum with bands at 2091 and 2023 cm⁻¹ (Figure 11). The spectrum measured at 175 °C is similar to that characterizing the sample containing clusters that had been decarbonylated in He at 60 °C. Recarbonylation of the sample that had been decarbonylated in H₂ at 275 °C resulted in a broad ν_CO band at 2057 cm⁻¹, which is similar to that characterizing CO adsorbed on supported platinum particles with a mean diameter of about 2 nm (Figure 12).

Oxidation of [PtRh₅(CO)₁₅]⁻ on MgO. Treatment of the MgO-supported clusters in O₂ resulted in the disappearance of the band at 1814 cm⁻¹ (Figure 13). The terminal carbonyl region included only two absorptions, at 2086 and 2014 cm⁻¹

MgO-Supported PtRh Clusters

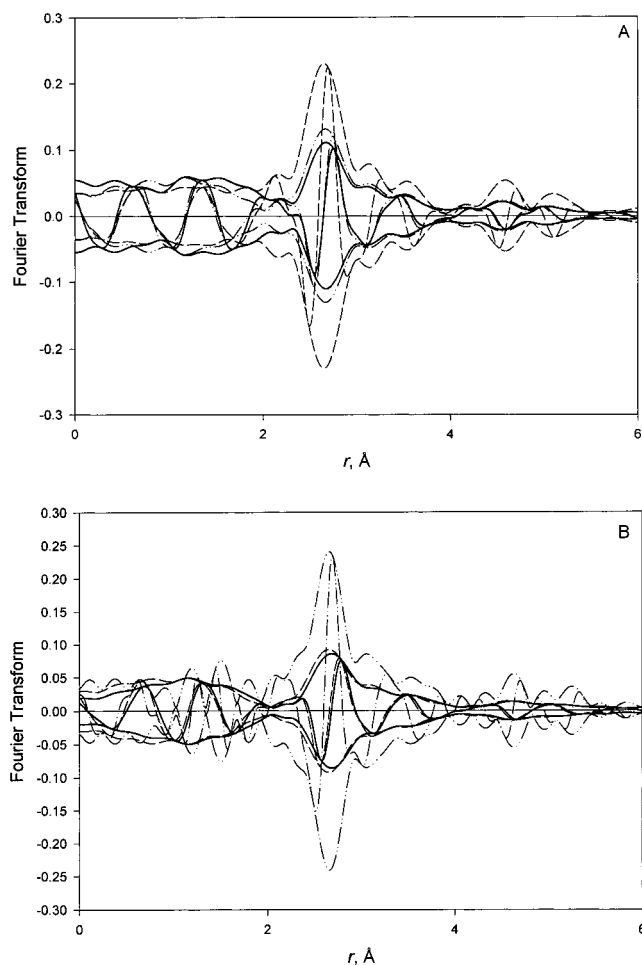*J. Phys. Chem. B, Vol. 102, No. 44, 1998* **8777**

Figure 8. Comparison of the Rh K-edge X-ray absorption data characterizing supported PtRh samples with different nuclearities: (A) magnitude of the Fourier transform (unweighted, Rh−Rh phase- and amplitude-corrected, $\Delta k = 4.1-12$) of EXAFS data characterizing the sample formed by treatment of the sample prepared by removal of solution from the slurry containing MgO and $[PtRh_5(CO)_{15}]^-$ in He at 125 °C (solid line), 175 °C (dotted−dashed line), and 400 °C (dashed line). (B) Magnitude of the Fourier transform (unweighted, Rh−Rh phase- and amplitude-corrected, $\Delta k = 4.1-12$ Å^{-1}) of EXAFS data characterizing the samples formed by treatment of $[PtRh_5(CO)_{15}]^-$/MgO in H$_2$ at 125 °C (solid line), 200 °C (dashed line), and 275 °C (dotted−dashed line).
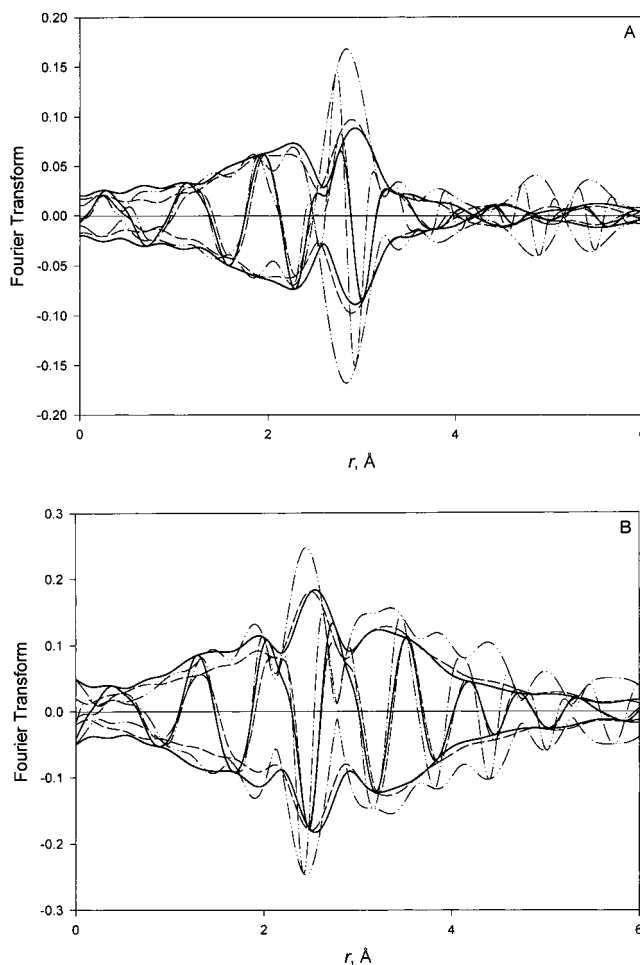
Figure 9. Comparison of the Pt L$_{III}$-edge X-ray absorption data characterizing supported PtRh samples with different nuclearities: (A) magnitude of the Fourier transform (unweighted, Pt−Rh phase and amplitude-corrected, $\Delta k = 3.7-11.5$ Å^{-1}) of EXAFS data characterizing the samples formed by treatment of the sample prepared by removal of solution from the slurry containing MgO and $[PtRh_5(CO)_{15}]^-$ in He at 125 °C (solid line), 175 °C (dashed line), and 400 °C (dotted−dashed line). (B) Magnitude of the Fourier transform (unweighted, Pt−Pt phase- and amplitude-corrected, $\Delta k = 3.7-11.5$ Å^{-1}) of EXAFS data characterizing the samples formed by treatment of the sample prepared by removal of solution from the slurry containing MgO and $[PtRh_5(CO)_{15}]^-$ in He at 125 °C (solid line), 175 °C (dashed line), and 400 °C (dotted−dashed line).

(Figure 13). When the temperature was raised to 175 °C, these bands disappeared and decarbonylation was complete.

Discussion

Evidence of $[PtRh_5(CO)_{15}]^-$ on MgO. The infrared data support the conclusion of Xu et al.[16] that $[PtRh_5(CO)_{15}]^-$ clusters were synthesized in solution and subsequently adsorbed on MgO. The Rh K-edge EXAFS data are in agreement with the conclusion, indicating a Rh−Rh contribution at a distance of 2.76 Å with a coordination number of 4 (Table 4). These values agree within the expected experimental errors (approximately ±2% and ±20%, respectively) with the expected values for $[PtRh_5(CO)_{15}]^-$ based on XRD data (2.77 Å and 3.2, respectively).

However, the Debye−Waller factor associated with the Rh−Rh contribution was found to be 0.0084 Å^2, which is large for supported metal carbonyl clusters, exemplified by $[Rh_6(CO)_{16}]$.[17] This value suggests that the rhodium-containing species were nonuniform, possibly consisting of variously distorted clusters

and/or more than one rhodium-containing species. Furthermore, because the Debye−Waller factor is so large, the Rh−Rh first-shell coordination number may be significantly overestimated (because in the data fitting this coordination number and the Debye−Waller factor are coupled parameters). Thus, the Rh K-edge data are consistent with the inference based on infrared spectroscopy that $[PtRh_5(CO)_{15}]^-$ was present on the MgO surface, but they also support the suggestion that this was not the only rhodium-containing surface species.

Consistent with the conclusion that the surface species included $[PtRh_5(CO)_{15}]^-$, the Pt L$_{III}$-edge EXAFS data characterizing the MgO-supported sample indicate the presence of both Pt−C and Pt−O contributions. Furthermore, a Pt−Rh contribution could be fitted (although the data are not sufficient to identify it with confidence), with a coordination number of 2.9 at a distance of 2.83 Å. Although these values are comparable to the values indicated by the X-ray diffraction data determined for crystalline $[PtRh_5(CO)_{15}]^-$ (4 and 2.79 Å, respectively),[15] the relatively low data quality and the relatively large errors in the values characterizing the Pt−Rh contribution imply that the
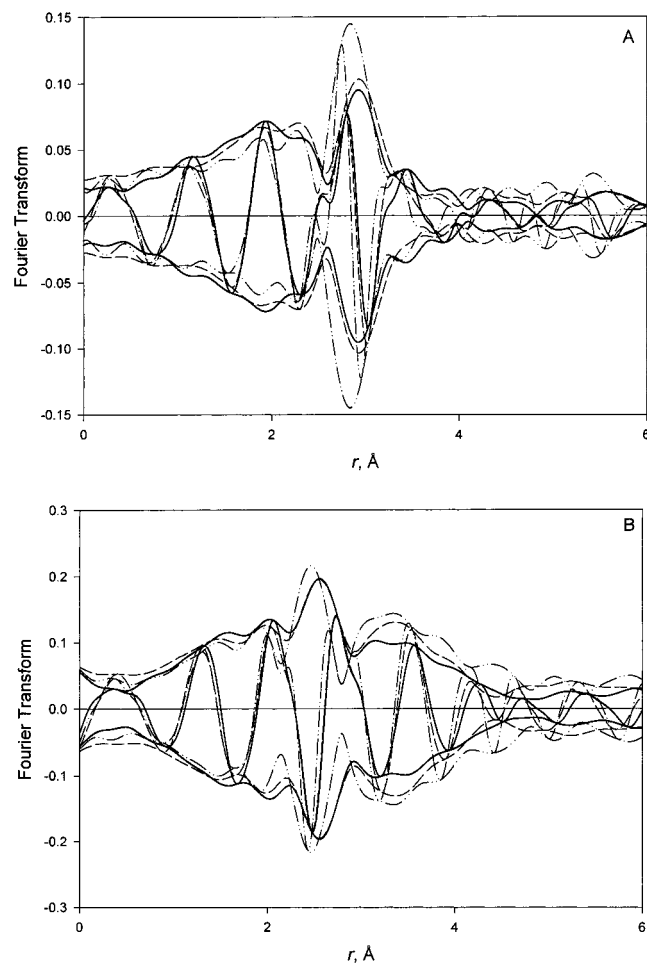
Figure 10. Comparison of the Pt L_{III}-edge X-ray absorption data characterizing supported PtRh samples with different nuclearities: (A) magnitude of the Fourier transform (unweighted, Pt−Rh phase and amplitude corrected, $\Delta k = 3.7-11.5$ Å^{-1}) of EXAFS data characterizing the samples formed by treatment of [PtRh$_5$(CO)$_{15}$]$^-$/MgO in H$_2$ at 125 °C (solid line), 200 °C (dashed line), and 275 °C (dotted−dashed line). (B) Magnitude of the Fourier transform (unweighted, Pt−Pt phase- and amplitude-corrected, $\Delta k = 3.7-11.5$ Å^{-1}) of EXAFS data characterizing the samples formed by treatment of [PtRh$_5$(CO)$_{15}$]$^-$/MgO in H$_2$ at 125 °C (solid line), 200 °C (dashed line), and 275 °C (dotted−dashed line).

EXAFS data alone are an insufficient basis for determining whether [PtRh$_5$(CO)$_{15}$]$^-$ was adsorbed intact on the MgO surface when the methanol was removed from the slurry. The value of the Debye−Waller factor (Table 4) characterizing the Pt−Rh contribution provides no additional insight because no suitable basis for comparison exists.

Thus, the EXAFS data are important in confirming the infrared data by being consistent with the presence of [PtRh$_5$(CO)$_{15}$]$^-$ on the MgO surface and in addition suggesting the presence of species besides [PtRh$_5$(CO)$_{15}$]$^-$.

The Rh K-edge XANES data also give evidence of the surface species other than the extractable clusters, which have been identified as [PtRh$_5$(CO)$_{15}$]$^-$. The greater white-line area in the XANES region of the X-ray absorption spectrum characterizing the MgO-supported bimetallic sample relative to that characterizing NaY zeolite-supported [Rh$_6$(CO)$_{16}$] (for which there is only little variation in the Rh−Rh bonding distances)[32,33] (Figure 5) indicates the presence of cationic rhodium species in the former sample. Candidate structures that might account for the XANES results include mononuclear rhodium complexes bonded to the MgO surface (e.g., rhodium subcarbonyls,
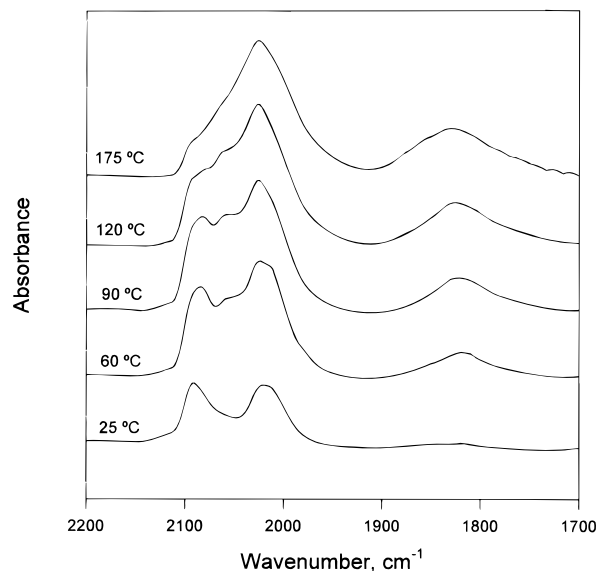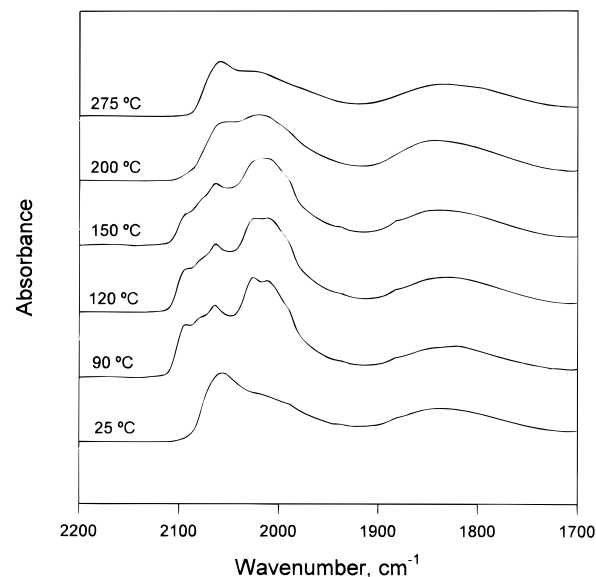

Figure 11. Infrared spectra of recarbonylation of the sample formed by decarbonylation of the sample prepared by removal of solution from the slurry containing MgO and [PtRh$_5$(CO)$_{15}$]$^-$ in He at 175 °C at the temperatures shown in CO at 1 atm.

Figure 12. Infrared spectra of recarbonylation of the sample formed by decarbonylation of the sample prepared by removal of solution from the slurry containing MgO and [PtRh$_5$(CO)$_{15}$]$^-$ in H$_2$ at 275 °C at the temperatures shown in CO at 1 atm.

Rh(CO)$_2$ or Rh(CO)$_3$),[34,35] as these would not have been extracted into solution as [PtRh$_5$(CO)$_{15}$]$^-$ was.

Because some of the clusters may have been oxidatively fragmented after being adsorbed on the MgO surface (by reaction, e.g., with surface OH groups) to give the rhodium subcarbonyls,[34,35] the resultant cationic species would be expected to be in close proximity to each other. Therefore, weak metal−metal interactions might be detected by EXAFS spectroscopy at both the Pt and Rh edges. However, the distances between the metal atoms would likely be influenced by the MgO surface structure and thus be nonuniform, consistent with the large Debye−Waller factor characterizing the Rh−Rh contribution (Table 4).

Because the rhodium XANES data indicate that some of the rhodium was present as cationic (and likely mononuclear) species, the question arises as to what fraction of the rhodium
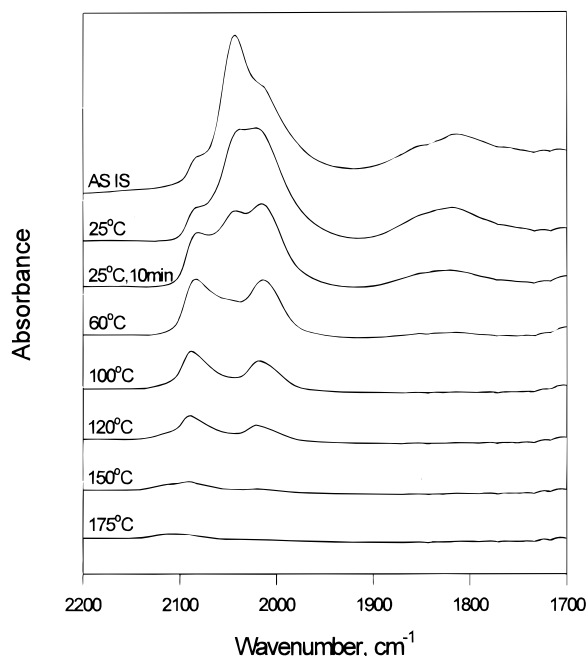
MgO-Supported PtRh Clusters

J. Phys. Chem. B, Vol. 102, No. 44, 1998 **8779**

Figure 13. Infrared spectra of the sample prepared by removal of solution from the slurry containing MgO and $[PtRh_5(CO)_{15}]^-$ and its subsequent treatments in O_2 at the temperatures shown.

was present in clusters. We can give only a rough approximation of this fraction based on the Pt−Rh coordination number (2.9) determined from the Pt L_{III}-edge EXAFS, which is less than the value determined by XRD (4). Assuming, for simplicity, that the metal was present either as $[PtRh_5(CO)_{15}]^-$ or as noncluster species, we estimate the fraction of the rhodium that remained intact in the form of these clusters as $N_{Pt−Rh}$(EXAFS)/$N_{Pt−Rh}$(XRD), where N refers to the coordination number. According to this rough estimate, at most 75% of the initial $[PtRh_5(CO)_{15}]^-$ clusters remained intact on the MgO surface after adsorption. [We based this estimate on the Pt-edge rather than the Rh-edge EXAFS data because experimental the Rh−Rh coordination number (4) is believed to be an overestimate, as stated above; the fact that this value is larger than the value expected on the basis of XRD (3.2) is consistent with our inference that the value is an overestimate.]

In summary, the infrared spectra of the supported clusters are consistent with the presence of $[PtRh_5(CO)_{15}]^-$ on the MgO surface. The EXAFS data are consistent with the presence of these clusters, and the XANES data indicate that these clusters were not the only species present on the MgO surface; the XANES data point to cationic rhodium species, but these are not identified with confidence. The implication of these results is that some of the $[PtRh_5(CO)_{15}]^-$ was adsorbed intact on MgO when the solvent methanol was removed and that some of these clusters reacted, possibly being oxidatively fragmented.

Pt−Rh Clusters and Aggregates Formed by Decarbonylation and Aggregation of MgO−Supported Metal Carbonyls. The infrared spectra give evidence of variously decarbonylated surface species; significant amounts of CO remained on the species formed by treatment of $[PtRh_5(CO)_{15}]^-$ on MgO in He at 125 °C, and only at 175 °C was the decarbonylation nearly complete (after 2 h) (Figure 6).

The EXAFS data provide structural information about the variously decarbonylated species, and the useful structural information is that characterizing the metal−metal contributions. The Rh K-edge EXAFS data provide the most accurate information about the structures of the clusters or aggregates

formed during the decarbonylation in He. The major metal−metal contribution was found to be Rh−Rh, with coordination numbers of 4.5 or 6 (with a Rh−Rh distance of about 2.67 Å) for samples treated in He at 125 °C or 175 °C, respectively (Figure 8A, Table 5). These results indicate metal clusters of about 6−10 atoms or 15−20 atoms each, respectively, on average.[36] Thus, the resultant clusters were small, but some aggregation accompanied the decarbonylation, with the degree of aggregation being negligible within experimental error at 125 °C and increasing with increasing temperature. We emphasize that the smallest clusters were at most only slightly larger, on average, than the six-atom frameworks of the precursor clusters. These are among the smallest bimetallic clusters reported.

The aggregates of metal formed in He at 400 °C are characterized by a Rh−Rh first-shell coordination number of about 10, indicating an average nuclearity of roughly 60 atoms.[36] Because the Rh−Pt contribution to the EXAFS signal was much smaller than the Rh−Rh contribution (indicating a small coordination number and possibly a large Debye−Waller factor), attempts to add this contribution to the fit of the data were unsuccessful.

The data show that the average Rh−Rh distance decreased as decarbonylation proceeded, with the maximum change being 0.1 Å. This is barely more than the estimated error in the Rh−Rh distance, ±2% or 0.06 Å, and the change may not be significant.

The qualitative trends in the Fourier transforms of the Pt L_{III}-edge EXAFS data characterizing the samples treated in He at 125, 175, and 400 °C show that the Pt−M coordination number (M = Rh or Pt) increased with increasing treatment temperature (Figure 9A). A strong Pt−Rh contribution is indicated by the data, at a distance of 2.76 Å, with a coordination number ranging from about 3.5 to 4.7. This trend showing the increase in the coordination number is supported by the qualitative trends in the magnitudes of the Fourier transforms. The results are important because they demonstrate the formation of bimetallic clusters (and aggregates), rather than segregated metals, in the sample. These results indicate that rhodium atoms were surrounded predominantly by other rhodium atoms rather than platinum atoms, whereas platinum atoms were surrounded predominantly by rhodium atoms.

The average Pt−Rh distance apparently decreased as decarbonylation took place, with the maximum change being 0.1 Å. Again, the change was barely more than the estimated experimental error in the distance and may not be significant.

Analysis of the EXAFS data characterizing each of the decarbonylated samples shows that there may be a Pt−Pt contribution, but it is small in comparison with the Pt−Rh contribution (Figures 9A and 10A). This result is consistent with the inference that the platinum in these samples was highly (perhaps even almost atomically) dispersed.

We also infer that the clusters and aggregates consisted predominantly of rhodium interiors with platinum on the surface or near the metal−support interface. The basis for this inference is the magnitudes of the coordination numbers stated in the preceding paragraphs: The increases in the Rh−Rh coordination number resulting from the treatments leading to decarbonylation and aggregation were much larger than the corresponding increases in the Pt−Rh coordination numbers, and the first-shell metal−metal coordination number of a surface atom can increase at most to about 9 (with about 6 atoms in the same plane as the surface atom and three atoms below) whereas that of a core atom can increase to about 12.

Decarbonylation of the supported metal carbonyl clusters in H_2 gave samples similar to those resulting from the treatment in He at similar temperatures. Decarbonylation in H_2 was nearly complete at 200 °C and complete at 275 °C. The Rh K-edge EXAFS data indicate that the Rh—Rh coordination number was roughly the same for the samples treated in H_2 at 125 and at 200 °C (about 5.5). These results indicate that the partially decarbonylated clusters formed had nuclearities of about 15 to 20 atoms each, on average.[36] Subsequent treatment in H_2 at 275 °C resulted in a large increase in the Rh—Rh coordination number, from about 5.5 to 9 (Table 5, Figure 8B). Treatment of the aggregates formed at 275 °C in H_2 at 400 °C did not cause further aggregation of the metal, as evidenced by the lack of a significant change in the Rh—Rh coordination number. These results indicate that the average nuclearities grew to about 50 atoms, on average.[36] We emphasize that all these aggregate nuclearities may be underestimated because of the suggested presence of mononuclear rhodium complexes (subcarbonyls).

The data characterizing the aggregates formed in H_2 show a smaller increase in the Pt—Rh coordination number than in the Rh—Rh coordination number (Table 5). Trends in the Pt—Rh and Rh—Rh coordination numbers parallel the trends observed for the supported aggregates formed in He, again implying that the locations of platinum and rhodium in the clusters were not random and consistent with enrichment of the aggregate surfaces in platinum.

We stress that the EXAFS data give no evidence of Pt—Pt contributions and hence no evidence of segregated platinum clusters or aggregates. However, if a small minority of the platinum atoms had segregated and aggregated into clusters, they would not have been detected because of the relative insensitiv of the EXAFS spectroscopy. What we can rule out is a substantial fraction of the platinum in the form of monometallic clusters or aggregates, but we cannot rule out the possibility of some segregated platinum along with segregated rhodium (as cationic species but perhaps even some aggregated species) in addition to the bimetallic species that are clearly demonstrated by the EXAFS data.

Comparison of the Debye—Waller factors characterizing the Rh—Rh contributions in the samples indicates the possibility of structural differences between the clusters or aggregates formed in He and those formed in H_2. Because the Debye—Waller factors characterizing the samples formed in He are smaller than those of the samples formed at the same temperature in H_2, we infer that the arrangement of metal in the bimetallic samples formed in He may be on average more uniform than the samples formed in H_2.

Comparison of MgO-supported PtRh Clusters and Aggregates Formed from [PtRh_5(CO)_15]^− with Conventionally Prepared Supported PtRh Clusters and Particles. The size and morphology of the PtRh clusters and aggregates reported here are different from what has been observed before. For example, Harada et al.[37] formed colloidal dispersions of polymer-protected PtRh particles having Pt:Rh atomic ratios of 1:1 or 1:4 by refluxing solutions of hexachloroplatinic(IV) acid and rhodium(III) chloride in ethanol/water in the presence of poly(N-vinyl-2-pyrrolidone). The bimetallic particles had diameters in the range of 20−70 Å, being similar in size to the largest aggregates formed in this work. On the basis of physical characterization data, Harada et al. concluded that their colloidal dispersions consisted predominantly of Pt—Rh alloys having platinum cores, in contrast to our samples. The differences between their samples and ours may be attributed both to the different Pt:Rh ratios and to the different preparation methods.

Tzou et al.[4] formed PtRh particles from platinum and rhodium salts supported on NaY zeolite. EXAFS data showed that in the calcined and reduced sample with a Pt:Rh atomic ratio of 1:2, platinum had no preference for association with one metal over the other. Cimini and Prins[5,6] used a similar method to make PtRh particles with Pt:Rh atomic ratios of 1:2 supported on NaY zeolite with various metal loadings. Traditional EXAFS spectroscopy showed that the particles were approximately spherical in structure, and Pt tended to bond to Pt and Rh tended to bond to Rh—in contrast to the results of Tzou et al.[4] Because EXAFS provides only average structural information, it did not lead to any conclusions about the compositional homogeneity of the particles.[5] However, by using QEXAFS (quick EXAFS), Cimini and Prins[6] were able to characterize the formation of the PtRh particles, demonstrating that, at low temperature, rhodium was first reduced to form monometallic clusters, and later, at higher temperatures, PtRh particles formed, characterized by Rh—Rh, Rh—Pt, Pt—Pt, and Pt—Rh contributions. The authors suggested that small bimetallic clusters moved through the zeolite channels and aggregated into particles. Thus, two kinds of particles were present, those having rhodium cores, which could be monometallic, and platinum-rich bimetallics. An important conclusion is that particles with nonhomogeneous compositions formed.[5,6] This result is in contrast to the results characterizing our rhodium-rich bimetallic clusters and aggregates, whereby the presence of Rh—Rh contributions and the lack of significant Pt—Pt contributions demonstrate more nearly homogeneous PtRh species.

Wang et al.[7] used [195]Pt NMR spectroscopy to characterize η-Al_2O_3-supported PtRh clusters with Pt:Rh atomic ratios ranging from 3:7 to 4:1, showing that poorly dispersed particles had platinum cores and highly dispersed particles contained both metals at their surfaces. These samples are also contrasted to ours, in which Pt—Pt bonds were not evident.

We suggest that the uniqueness of the structural properties of our samples is related to the synthesis method, whereby Pt—Rh bonds exist initially, so that the platinum and rhodium atoms are near each other on the support surface, even if some of the cluster frames have been broken up on the support (giving rhodium subcarbonyls, for example). In contrast, in the other syntheses referred to above, Pt—Rh bonds may not have formed prior to the calcination and reduction steps, and the metal cluster or particle compositions and morphologies may have been determined more by random mixing processes or even thermodynamic stability considerations.

Conclusions

$[PtRh_5(CO)_{15}]^−$ was formed in a slurry with MgO powder and adsorbed on the MgO surface when the solvent was removed. Infrared spectroscopy and EXAFS spectroscopy show that these clusters were present intact on the MgO surface. XANES data indicate that other species were also present. PtRh clusters and aggregates formed from these precursors as a result of treatment in He or H_2. The supported metal carbonyls were completely decarbonylated at 175 °C when treated in He and at 275 °C when treated in H_2. The decarbonylation processes were accompanied by aggregation of the metals, but low-temperature treatments gave supported clusters with about 10 atoms or fewer each, on average. The supported clusters and aggregates were found by EXAFS spectroscopy to be bimetallic; there is no evidence of segregation of the two metals in the clusters or aggregates. The data indicate that the clusters and aggregates consisted of rhodium-rich cores with surfaces enriched in platinum.

MgO-Supported PtRh Clusters

J. Phys. Chem. B, Vol. 102, No. 44, 1998 **8781**

References and Notes

(1) Oh, S. H.; Carpenter, J. E. *J. Catal.* **1986**, 98, 178.

(2) Sinfelt, J. H. U.S. Patent 3953368, 1976.

(3) Kluksdahl, H. E. U.S. Patent 3415737, 1968.

(4) Tzou, M. S.; Asakura, K.; Yamazaki, Y.; Kuroda, H. *Catal. Lett.* **1991**, *11*, 33.

(5) Cimini, F.; Prins, R. *J. Phys. Chem. B* **1997**, *101*, 5277.

(6) Cimini, F.; Prins, R. *J. Phys. Chem. B* **1997**, *101*, 5285.

(7) Wang, Z.; Ansermet, J.-P.; Slichter, C. P.; Sinfelt, J. H. *J. Chem. Soc., Faraday Trans. 1* **1988**, *84* (11), 3785.

(8) Wang, T.; Schmidt, L. D. *J. Catal.* **1981**, *70*, 187.

(9) Wang, T.; Schmidt, L. D. *J. Catal.* **1980**, *66*, 301.

(10) Braunstein, P.; Rose, J. In *Catalysis by Di- and Polynuclear Metal Cluster Complexes*; Adams, R. D., Cotton, F. A., Eds.; Wiley-VCH: New York, 1998; p 443.

(11) Shirai, M.; Yang, O.-B.; Weber, W. A.; Gates, B. C. 1998. Manuscript to be published.

(12) Fumagalli, A. *Mater. Chem. Phys.* **1991**, *29*, 211.

(13) Fumagalli, A.; Martinengo, S.; Chini, P.; Galli, D.; Heaton, B. T.; Pergola, R. D.; *Inorg. Chem.* **1984**, *23*, 2947.

(14) Fumagalli, A.; Martinengo, S.; Galli, D.; Albinati, A.; Ganazzoli, F. *Inorg. Chem.* **1989**, *28*, 2476.

(15) Fumagalli, A.; Martinengo, S.; Chini, P. *J. Chem. Soc., Chem. Commun.* **1978**, 195.

(16) Xu, Z.; Kawi, S.; Rheingold, A. L.; Gates, B. C. *Inorg. Chem.* **1994**, *33*, 4415.

(17) Weber, W. A.; Gates, B. C. *J. Phys. Chem. B* **1997**, *101*, 10423.

(18) Alexeev, O.; Kawi, S.; Shelef, M.; Gates, B. C. *J. Phys. Chem. B* **1996**, *100*, 253.

(19) Rehr, J. J.; Mustre de Leon, J.; Zabinsky, S. I.; Albers, R. C. *J. Am. Chem. Soc.* **1991**, *113*, 5135.

(20) Teo, B.-K. *J. Am. Chem. Soc.* **1981**, *103*, 3990.

(21) Duivenvoorden, F. B. M.; Koningsberger, D. C.; Uh, Y. S.; Gates, B. C. *J. Am. Chem. Soc.* **1986**, *108*, 6254.

(22) van Zon, F. B. M.; Maloney, S. D.; Gates B. C.; Koningsberger, D. C. *J. Am. Chem. Soc.* **1993**, *115*, 10317.

(23) van Zon, J. B. A. D. Ph.D. Dissertation, Eindhoven University of Technology, The Netherlands, 1988.

(24) van Zon, J. B. A. D.; Koningsberger, D. C.; van't Blik, H. F. J.; Sayers, D. E. *J. Chem. Phys.* **1985**, *82*, 5742.

(25) Wyckoff, R. W. G. *Crystal Structures*, 2nd ed.; Wiley: New York, 1963; Vol. 1, p 10.

(26) Coey, J. M. D. *Acta Crystallogr.* **1970**, *B26*, 1876.

(27) Mason, R.; Rae, A. I. M. *J. Chem. Soc. A* **1968**, 778.

(28) Trömel, M.; Lupprich, E. *Z. Anorg. Chem.* **1975**, *414*, 160.

(29) Churchill, M. R.; Hutchinson, J. P. *Inorg. Chem.* **1978**, *17*, 3528.

(30) Koningsberger, D. C.; Prins, R. *X-ray Absorption: Principles, Applications, Techniques of EXAFS, SEXAFS, and XANES.;* Wiley: New York, 1988; p 395.

(31) Kirlin, P. S.; van Zon, F. B. M.; Koningsberger, D. C.; Gates, B. C. *J. Phys. Chem.* **1990**, *94*, 8439.

(32) Weber, W. A. Ph.D. Dissertation, University of California, Davis, 1998.

(33) Corey, E. R.; Dahl, L. F.; Beck, W. *J. Am. Chem. Soc.* **1963**, *85*, 1202.

(34) Rao, L.-F.; Hwang, S.-J.; King, T. S.; Pruski, M. *J. Phys. Chem.* **1996**, *100*, 5668.

(35) Lamb, H. H.; Gates, B. C.; Knözinger, H. *Angew. Chem., Int. Ed. Engl.* **1988**, *27*, 1127.

(36) Kip, B. J.; Duivenvoorden, F. B. M.; Koningsberger, D. C. *J. Catal.* **1987**, *105*, 26.

(37) Harada, M.; Asakura, K.; Toshima, N. *J. Phys. Chem.*, **1994**, *98*, 2653.

(38) Vaarkamp, M.; Linders, J. C.; Koningsberger, D. C. *Phys. B* **1995**, *209*, 159.